Thermal stitching: Combining the advantages of different quantum fermion solvers

Justin C. Smith[1,2] and Kieron Burke[2,3]
[1]*Department of Mathematics, University of California, Los Angeles, California 90095, USA*
[2]*Department of Physics and Astronomy, University of California, Irvine, California 92697, USA*
[3]*Department of Chemistry, University of California, Irvine, California 92697, USA*

(Received 9 January 2018; published 27 August 2018)

For quantum fermion problems, many accurate solvers are limited by the temperature regime in which they can be usefully applied. The Mermin theorem implies the uniqueness of an effective potential from which both the exact density and free energy at a target temperature can be found, via a calculation at a different, reference temperature. We derive exact expressions for both the potential and the free energy in such a calculation and introduce three controllable approximations that reduce the cost of such calculations. We illustrate the effective potential and its free energy, and test the approximations, on the asymmetric two-site Hubbard model at finite temperature.

DOI: 10.1103/PhysRevB.98.075148

I. INTRODUCTION

The fermionic quantum problem occurs in many areas of physics and is notoriously difficult to solve [1]. It is at the heart of all electronic structure problems, and so solution methods have enormous impact in condensed matter physics, quantum chemistry, materials science, and beyond [2]. Over decades, many diverse approaches have been developed and refined [3]. In almost all cases, there are tradeoffs between accuracy, computational cost, and domain of applicability. Some techniques are almost solely designed to work on finite systems at zero temperature (e.g., many *ab initio* quantum chemical approaches), while others are extremely general but costs become prohibitive as the temperature lowers (e.g., path integral Monte Carlo (PIMC) [4,5]). A collection of high-accuracy methods were recently benchmarked on strongly-correlated lattice models [6]. On the other hand density-functional methods are relatively inexpensive but require an uncontrolled approximation to the exchange-correlation (XC) energy. Recently, density functional theory (DFT) methods have enjoyed considerable success in being applied at temperatures relevant to warm dense matter (WDM), a phase of matter with properties of solids and plasmas [7], such as occurs in fusion experiments and planetary cores [8–20].

The central question addressed in this work is: Can a quantum fermion solver be run at one temperature (the reference temperature) to yield results at some other temperature (the target temperature)? Such a scheme could be applied to many diverse combinations of calculations. In the examples above, it could be used to bootstrap PIMC calculations to lower temperatures, quantum chemical calculations to finite temperatures, or to combine DFT methods with more accurate solvers for WDM [21–23]. Our work is compatible with other approaches such as the formulation by Alavi and coworkers [24]. Any two methods can be combined using our stitching method.

We show that the answer is in principle yes, at least for extracting the free energy and density. Inspired by Ref. [25], we use the Mermin theorem [26] to define a unique effective one-body potential from which, with an accurate quantum solver, we can extract the target quantities. We derive the relevant formulas for a finite-temperature Kohn-Sham treatment. We identify three useful, controllable approximations that make extraction of the target free energy easier in practice. Finally, we illustrate the relevant exact quantities and test the approximations on the finite-temperature asymmetric Hubbard dimer.

Our formulas are general for any quantum fermion problem, but we will discuss WDM simulations as an example. Mermin generalized the Hohenberg-Kohn theorem [27] to nonzero temperatures at thermal equilibrium [26]. Thermal DFT became a popular tool of plasma physics in subsequent decades [28–30]. The advent of accurate ground-state approximations and robust codes led to many recent successes of thermal DFT [12,13,18,19,31–36]. For greater reliability and higher accuracy, but at much higher computational cost, PIMC simulations are used [4,5,37–41].

Thermal DFT is made computationally tractable by the use of a noninteracting potential $v_s^\tau(\mathbf{r})$ that yields the interacting density, $n^\tau(\mathbf{r})$, at temperature τ. This Mermin-Kohn-Sham (MKS) system is exact in principle but in practice requires approximations to the XC free energy, $A_{\rm xc}^\tau[n]$, as a functional of the density [42]. Most WDM simulations use the zero-temperature approximation [43], which replaces $A_{\rm xc}^\tau[n]$ by $E_{\rm xc}[n]$, an approximation to the ground-state XC energy [44] but used in the MKS equations. An alternative is to use the thermal local density approximation, where a parametrization of the XC free energy of the homogeneous electron gas is used to approximate $A_{\rm xc}^\tau[n]$ [40,45–47]. Thermal generalized gradient approximations [48,49] have also been suggested.

II. THEORY AND RESULTS

Begin with the Mermin-Kohn-Sham scheme. The equations are identical to those of the ground state,

$$\left\{-\tfrac{1}{2}\nabla^2 + v_s^\tau(\mathbf{r})\right\}\phi_i^\tau(\mathbf{r}) = \epsilon_i^\tau\,\phi_i^\tau(\mathbf{r}), \tag{1}$$

with the exception that the density is found by thermally occupying the MKS orbitals:

$$n^\tau(\mathbf{r}) = \sum_i f_i^\tau \left|\phi_i^\tau(\mathbf{r})\right|^2, \tag{2}$$

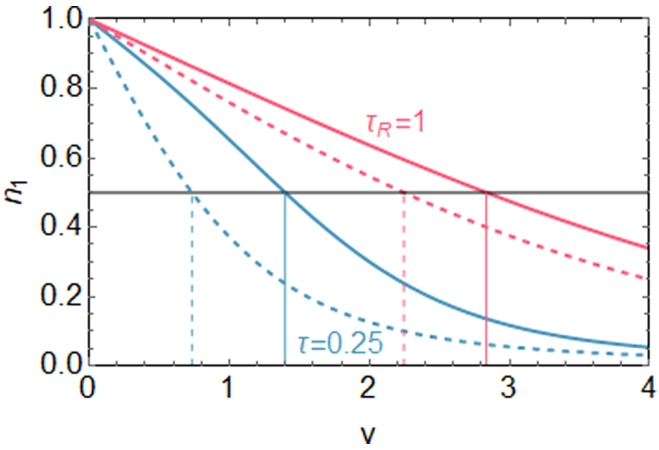

FIG. 1. n_1 vs x at $\tau = 0.25$ (blue) and $\tau = 1$ (red). Solid lines are $U = 1$ and dashed are noninteracting, $U = 0$. The intersections with the horizontal line at $n_1 = 0.5$ give the v values that yield $n_1 = 0.5$ for the given temperature and interaction.

where the occupations are Fermi factors at temperature τ. $v_s(\mathbf{r})$ is defined by Eqs. (1) and (2). Write the free energy in terms of the MKS components:

$$A[v] = \min_n \left(T_s^\tau[n] - \tau S_s^\tau[n] + U[n] + A_{XC}^\tau[n] + \mathcal{I}[nv]\right), \tag{3}$$

where T_s^τ is the MKS noninteracting kinetic energy at temperature τ, S_s^τ is the corresponding entropy, U is the Hartree energy, and we introduced

$$\mathcal{I}[f] = \int d^3r\, f(\mathbf{r}) \tag{4}$$

to represent the external potential energy. Writing

$$v_s^\tau(\mathbf{r}) = v(\mathbf{r}) + v_H[n](\mathbf{r}) + v_{XC}^\tau[n](\mathbf{r}), \tag{5}$$

and identifying $v_H(\mathbf{r})$ as the Hartree potential and $v_{XC}^\tau(\mathbf{r})$ as the functional derivative of A_{XC}^τ, the self-consistent solution of the MKS equations finds the minimum density in Eq. (3).

We demonstrate this with a simple exact model which is a crude representation of a chemical bond. The asymmetric Hubbard dimer has been used to test and understand many flavors of DFT including ground-state [50,51], time-dependent [52–56], ensemble [57], thermal [43,58,59], and DFT-like methods [60]. Here, the Hubbard dimer is used to illustrate the exact properties of the stitching potential and simple approximations for extracting the free energy. In no significant sense does it mimic the complexities of realistic WDM simulations. Its Hamiltonian is

$$\hat{H} = -t \sum_\sigma (\hat{c}_{1\sigma}^\dagger \hat{c}_{2\sigma} + \text{H.c.}) + \sum_i (U \hat{n}_{i\uparrow}\hat{n}_{i\downarrow} + v_i \hat{n}_i), \tag{6}$$

where $\hat{c}_{i\sigma}^\dagger(\hat{c}_{i\sigma})$ is the electron creation (annihilation) operator and $\hat{n}_{i\sigma} = \hat{c}_{i\sigma}^\dagger \hat{c}_{i\sigma}$ is the number operator, t is the electron hopping, U is the Coulomb repulsion, and v_i is the onsite potential. We choose $v_1 + v_2 = 0$, define $v = v_2 - v_1$, and $2t = 1$. In lattice DFT the site occupations [61], n_1 and n_2, are analogous to the density. We work at half filling ($\langle N \rangle = 2$) which restricts $\mu = U/2$ to maintain particle-hole symmetry. Figure 1 shows exact thermal calculations. The solid red line is the density on site 1 as a function of the onsite potential v, for a relatively hot temperature ($\tau = 1$). The Mermin theorem guarantees its monotonicity. The dashed red line is the same map but for tight binding, i.e., $U = 0$. Thus, for a system with $v = 2.834$ (marked by solid red vertical line), $n = 0.5$ at $\tau = 1$. The MKS potential is $v_s^\tau = 2.246$ (vertical dashed red line), and the difference is the HXC contribution. The blue lines denote the same things at a lower temperature, $\tau = 1/4$.

Mermin proved that in the grand canonical ensemble for fixed temperature and chemical potential there exists a one-to-one correspondence between the external potential and electronic density for given particle statistics, interaction, and temperature, τ [26]. Assuming v representability, the map $\bar{n}^\tau[v](\mathbf{r})$ is invertible and the map $v^\tau[n](\mathbf{r})$ exists. Note that the former is a potential functional (denoted by a bar), while the latter is a density functional. Assuming noninteracting representability, we can write

$$\bar{v}_s^\tau[v](\mathbf{r}) = \left(n_s^\tau\right)^{-1}[\bar{n}^\tau[v]](\mathbf{r}). \tag{7}$$

This compact expression is the map between the one-body potential of the interacting problem and its MKS equivalent, i.e., this is the MKS potential as a functional of the one-body potential of the interacting problem, which is different from its density dependence as expressed in Eq. (5).

For any system, we can define an effective thermal potential (ETP), $\bar{v}_\tau^{\tau_R}(\mathbf{r})$, as the one-body potential that yields the exact density at τ by performing a calculation at τ_R. This is unique by Mermin's theorem and can be written

$$\bar{v}_\tau^{\tau_R}[v](\mathbf{r}) = (n^{\tau_R})^{-1}[n^\tau[v]](\mathbf{r}). \tag{8}$$

A noninteracting map is defined in the same way. Figure 1 also illustrates the ETP logic. The horizontal line is $n_1 = 0.5$ and everywhere that it intersects a curve corresponds to the potential that yields $n_1 = 0.5$ for the given temperature and interaction strength. Thus $\bar{v}_\tau^{\tau_R}[v]$ is given by the dependence of the blue vertical line on the red one, with an analogous noninteracting version with dashed vertical lines. This effective potential has some specific symmetry properties, namely

$$\bar{v}_{\tau_R}^\tau\left[\bar{v}_\tau^{\tau_R}[v]\right](\mathbf{r}) = \bar{v}_\tau^\tau[v](\mathbf{r}) = v(\mathbf{r}). \tag{9}$$

We wish to derive the ETP for an MKS calculation, using some $\tilde{v}_{XC}^\tau[n](\mathbf{r})$, where this XC potential could be approximate or exact. To do this, we must use the concept of a ffunctional [62]. A functional is a function of a function, whereas a ffunctional is a functional of a functional. Identify $n^\tau\{\tilde{v}_{XC}\}[v](\mathbf{r})$ as the density at temperature τ found by solving the MKS equations with $\tilde{v}_{XC}^\tau[n](\mathbf{r})$. Then

$$\bar{v}_\tau^{\tau_R}[v](\mathbf{r}) = v_s^{\tau_R}[n^\tau\{\tilde{v}_{XC}\}[v]](\mathbf{r}) - v_{HXC}^{\tau_R}[n^\tau\{\tilde{v}_{XC}\}[v]](\mathbf{r}). \tag{10}$$

This result shows how to construct an approximate ETP from a MKS calculation at different temperatures with a given XC potential. Simply calculate the density from MKS at the desired temperature, find what noninteracting potential yields that density at the reference temperature, and subtract off the approximate HXC potential evaluated at the reference temperature. In Fig. 1, the first term is the MKS contribution (vertical dashed blue line), while the second is the HXC correction (difference between solid and dashed vertical blue lines). Thus a DFT approximation might be used to generate PIMC-quality densities at τ by performing PIMC calculations

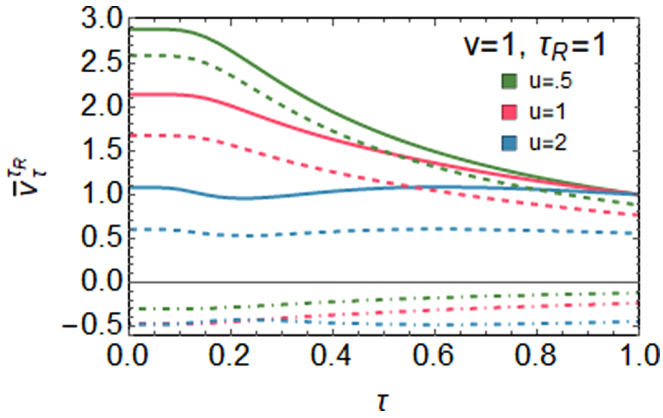

FIG. 2. Effective thermal potential for $v = 1$ and $\tau_R = 1$ for various correlation strengths. Solid curves are interacting, dashed are noninteracting, and dot-dashed is Hxc. All calculations yield $\bar{v}_{\mathrm{Hxc},\tau}^{\tau_R} \leqslant 0$.

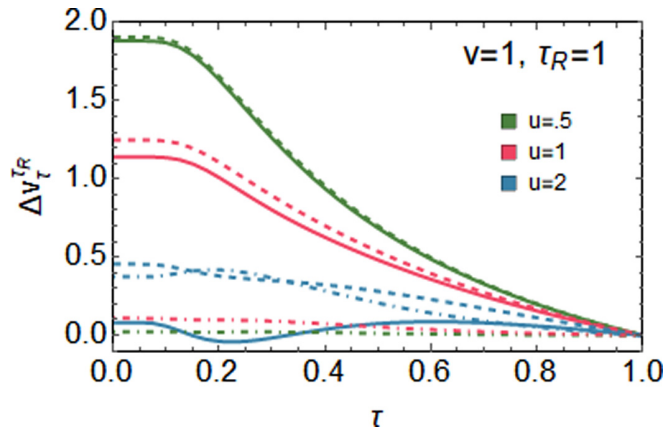

FIG. 3. Same as previous figure, but now for the difference between ETP and its reference.

only at τ_R. This is a key result: Thermal stitching enables computationally tractable explorations of complex physics by combining the capabilities of multiple fermionic solvers. Our result satisfies several conditions: (i) If the exact XC functional is used, the exact $n^\tau(\mathbf{r})$ is found; (ii) if an approximate XC and the resulting ETP are used in an MKS calculation, the corresponding self-consistent approximate density is found; (iii) if the temperatures are equal, the exact result is recovered. But the symmetry of Eq. (9) is lost with an approximate XC.

In Fig. 2, we plot the exact ETP, for a system with $v = 1$. Green denotes weak correlation. The solid line is the interacting curve, which varies strongly with temperature (and approaches v as $\tau \to \tau_R$). The dashed line is the MKS ETP, which mimics the interacting curve closely and approaches the MKS potential at τ_R. The dot-dashed line is the HXC contribution, which is smoother and relatively small, suggesting it might be amenable to approximation.

We also show what happens as we increase the correlation to $u = 1$ (red) and $u = 2$ (blue). For moderate correlation, the effects are similar but larger. But for strong correlation temperature dependence is mitigated, the HXC contribution is comparable to the MKS piece, and small errors in approximations are less likely to be forgiven.

In Fig. 3, we plot the difference between the ETP and its reference value (v and v_s^τ for interacting and noninteracting, respectively), showing that the HXC contributions are now even smaller. They remain monotonic when correlation is weak or moderate and vanish rapidly as $\tau \to \tau_R$. This strongly suggests that approximating the XC contribution to the thermal correction potential with a local or semilocal density functional approximation should introduce relatively little error in the density for weakly correlated systems. For strong correlation, the HXC contribution is of the same order as the MKS potential, develops nonmonotonic behavior, and vanishes much more slowly with temperature. A semilocal density approximation might introduce much larger errors in this case.

Although the density is important, greatest interest is often in the free energy and related properties. Thus we need to generate accurate free energies from our formulas. We begin with a recently proven formula [63] from a generalization of potential functional theory [62,64,65] to the grand canonical ensemble. Assume the energy components are known exactly for some given reference potential, v_0, and write $v^\lambda(\mathbf{r}) = v_0(\mathbf{r}) + \lambda\Delta v(\mathbf{r})$, where $\Delta v(\mathbf{r}) = v(\mathbf{r}) - v_0(\mathbf{r})$. The free energy of the system is then:

$$A^\tau[v] = A_0^\tau + \mathcal{I}[\bar{n}^\tau[v, \Delta v]\Delta v], \tag{11}$$

where $\bar{n}^\tau[v, \Delta v] = \int_0^1 d\lambda\, n^\tau[v^\lambda](\mathbf{r})$. Here 0 subscripts denote quantities for the reference potential. We find, exactly, for the deviation from the reference A_{HXC}^τ:

$$\Delta A_{\mathrm{HXC}}^\tau[\Delta v] = \mathcal{I}[\bar{n}^\tau[v, \Delta v]\Delta v] - \mathcal{I}\left[\bar{n}_s^\tau\left[v_s^\tau, \Delta v_s^\tau\right]\Delta v_s^\tau\right] + \mathcal{I}\left[n^\tau[v]v_{\mathrm{HXC}}^\tau - n_0^\tau[v_0]v_{\mathrm{HXC},0}^\tau\right]. \tag{12}$$

The derivation of Eq. (12) is given in the Supplemental Material [66].

To illustrate the value of a well-chosen reference, in Fig. 4, we plot the free energy versus temperature using Eq. (11) with the reference potential set to 0, i.e., the symmetric dimer. We see that the deviation from the reference is an order of magnitude smaller than the reference value, making it easier to approximate. Note that our reference temperature is twice as high as before, but even at half its value, the deviation in the free energy from the reference is difficult to detect.

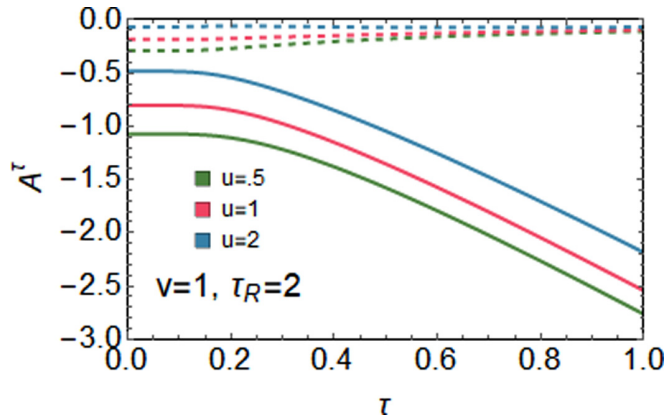

FIG. 4. Temperature dependence of the free energy and its deviation from reference for the same systems as in the previous figures.

In principle, Eq. (12) is sufficient to extract the free energy from a thermal-stitching calculation. Although the input densities are required at the target temperature τ, these can all be found from calculations at the reference temperature. The last term in Eq. (12) is straightforward, but the first involves averages over λ that are cumbersome since the ETP must be evaluated for every λ. The last step is to derive a controlled approximation that yields an accurate expression using only quantities evaluated at τ_R.

We make three distinct approximations. In the first, we note that the exact formula requires finding $n_s^\tau[v_{s,0}+\lambda\Delta v_s](\mathbf{r})$ which, in general, is not equal to $n^\tau[v_0+\lambda\Delta v](\mathbf{r})$. However, they match at $\lambda=0$ and $\lambda=1$, and nearly agree everywhere for weak interaction, so we expect

$$n_s^\tau[v_{s,0}+\lambda\Delta v_s](\mathbf{r}) \approx n^\tau[v_0+\lambda\Delta v](\mathbf{r}) \tag{13}$$

to produce little error. A second approximation is to approximate each coupling-constant integral by a two-point formula:

$$\bar{n}^\tau[v,\Delta v](\mathbf{r}) \approx \tfrac{1}{2}(n^\tau[v_0](\mathbf{r})+n^\tau[v](\mathbf{r})). \tag{14}$$

With these Eq. (12) simplifies to

$$\begin{aligned}\Delta A_{xc}^{\tau,\mathrm{app}}[v] = {}& \mathcal{I}\big[(n^\tau[v]-\bar{n}^\tau[v])v_{xc}^\tau\big] \\ & -\mathcal{I}\big[(n^\tau[v_0]-\bar{n}^\tau[v])v_{xc,0}^\tau\big],\end{aligned} \tag{15}$$

with the Hartree contributions canceling on both sides (see Supplemental Material for derivation [66]). Inserting the ETP is now simple:

$$\begin{aligned}\Delta A_{xc}^{\tau,\mathrm{app}}[v] = {}& \mathcal{I}\Big[\big(n^{\tau_R}\big[\tilde{v}_\tau^{\tau_R}[v]\big]-\bar{n}^{\tau_R}\big[\tilde{v}_\tau^{\tau_R}[v]\big]\big)v_{xc}^\tau\Big] \\ & -\mathcal{I}\Big[\big(n^{\tau_R}\big[\tilde{v}_\tau^{\tau_R}[v_0]\big]-\bar{n}^{\tau_R}\big[\tilde{v}_\tau^{\tau_R}[v]\big]\big)v_{xc,0}^\tau\Big].\end{aligned} \tag{16}$$

This formula yields (approximately) the XC free energy at τ using only densities from τ_R, ETPs, and the XC potential at τ, which can be extracted via a MKS inversion from the accurate density at τ, i.e., Eq. (7), and subtraction of the external and Hartree potentials.

Although Eq. (16) contains only quantities evaluated at the reference temperature, as required, they are awkward because the reference potentials and densities must be found for many values of λ, and then averaged over the coupling constant. This process can be simplified by a linear approximation for the ETP:

$$\begin{aligned}\tilde{v}_\tau^{\tau_R}[v^\lambda](\mathbf{r}) &= \tilde{v}_\tau^{\tau_R}[v_0+\lambda(v-v_0)](\mathbf{r}) \\ &\approx \tilde{v}_\tau^{\tau_R}[v_0](\mathbf{r})+\lambda\big(\tilde{v}_\tau^{\tau_R}[v](\mathbf{r})-\tilde{v}_\tau^{\tau_R}[v_0](\mathbf{r})\big),\end{aligned} \tag{17}$$

which should be an excellent approximation for weak correlation.

In Fig. 5, we plot correlation energies exactly, approximately but doing the coupling-integral in Eq. (16) explicitly, and approximately with Eq. (17) to approximate the coupling integrations. Using Eq. (16) introduces small errors for low temperatures but these quickly diminish as temperature increases. Interestingly, they seem no worse when correlations are stronger. Linearizing the potential slightly worsens the results but makes a smaller error than already present in Eq. (16). This error also diminishes rapidly with increasing temperature. Correlation becomes a relatively smaller part of the total free energy as temperature increases [43]. The majority of the contribution to the correlation free energy is in the reference term with similar behavior in the correction term as seen for the total free energy, and we make only a small error in approximating the correction.

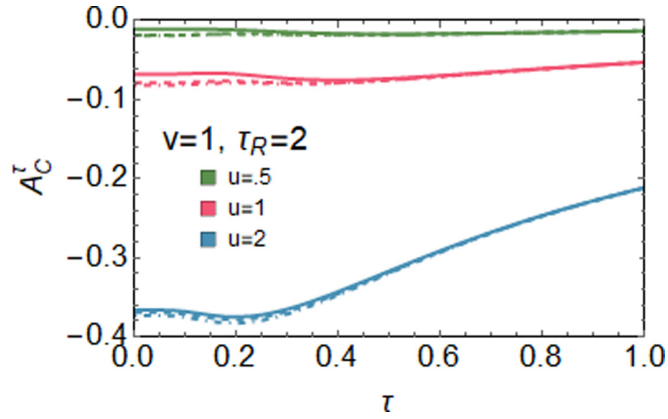

FIG. 5. Correlation free energy from ETP for the same system as previous figures. Solid is exact, dashed is from Eq. (16), and dot-dashed includes the further approximation of Eq. (17).

III. CONCLUSION

In this paper we presented a formally exact method for determining electronic properties at temperature τ using a calculation at temperature τ_R. To do so, we defined an ETP which yields the exact density at τ of a given system. We also derived an approximate formula from potential functional theory for the exchange-correlation free energy that uses only the ETP. We applied simple approximations to this equation to put it in a more elegant form and to make it only require the ETP. All of this was illustrated using the asymmetric Hubbard dimer.

We conclude with suggestions for approximations and future work. For extended matter in WDM simulations, an obvious reference potential is the uniform electron gas with the average electronic density of the entire system. The free energy of this system is well known [23,45,46,67,68]. Then the coupling-constant integral connects local differences in the potential from its average value. Equation (10) would also be tested with, e.g., a zero-temperature GGA approximation for the MKS approximation. This yields an approximate density at τ and the corresponding HXC approximation at τ_R. Then the same MKS code could be used to find the corresponding MKS potential at τ_R, by adjusting $v_s^{\tau_R}(\mathbf{r})$ until $\tilde{n}^\tau(\mathbf{r})$ is found. These yield the approximation to the ETP to be used in an accurate quantum solver at τ_R. Note that one could imagine this as the first step in an iterative procedure in which the

output approximate density at τ is used in place of the MKS approximate density. This would unbalance the use of DFT in the formula which might in fact worsen the results. Only practical calculations can tell. Additional tests include long Hubbard chains, more complicated lattices, and atoms. These tests can further demonstrate the theory's applicability and accuracy.

ACKNOWLEDGMENTS

The authors acknowledge support from the U.S. Department of Energy (DOE), Office of Science, Basic Energy Sciences under Award No. DE-FG02-08ER46496. J.C.S. acknowledges support through the NSF Graduate Research fellowship program under Award No. DGE-1321846.

[1] P. A. M. Dirac, Quantum mechanics of many-electron systems, Proc. R. Soc. London, Ser. A **123**, 714 (1929).

[2] A. Pribram-Jones, D. A. Gross, and K. Burke, Dft: A theory full of holes?Annu. Rev. Phys. Chem. **66**, 283 (2015).

[3] R. M Martin, L. Reining, and D. M Ceperley, *Interacting Electrons* (Cambridge University Press, Cambridge, UK, 2016).

[4] D. M. Ceperley, Path integrals in the theory of condensed helium, Rev. Mod. Phys. **67**, 279 (1995).

[5] K. P. Driver and B. Militzer, All-Electron Path Integral Monte Carlo Simulations of Warm Dense Matter: Application to Water and Carbon Plasmas, Phys. Rev. Lett. **108**, 115502 (2012).

[6] M. Motta, D. M. Ceperley, G. Kin-Lic Chan, J. A. Gomez, E. Gull, S. Guo, C. A. Jiménez-Hoyos, T. Nguyen Lan, J. Li, F. Ma, A. J. Millis, N. V. Prokof'ev, U. Ray, G. E. Scuseria, S. Sorella, E. M. Stoudenmire, Q. Sun, I. S. Tupitsyn, S. R. White, D. Zgid, and S. Zhang (Simons Collaboration on the Many-Electron Problem), Towards the Solution of the Many-Electron Problem in Real Materials: Equation of State of the Hydrogen Chain with State-of-the-Art Many-Body Methods, Phys. Rev. X **7**, 031059 (2017).

[7] F. Graziani, M. P. Desjarlais, R. Redmer, and S. B. Trickey (eds.), *Frontiers and Challenges in Warm Dense Matter*, Lecture Notes in Computational Science and Engineering, Vol. 96 (Springer International Publishing, Basel, Switzerland, 2014).

[8] B. F Rozsnyai, J. R Albritton, D. A Young, V. N Sonnad, and D. A Liberman, Theory and experiment for ultrahigh pressure shock hugoniots, Phys. Lett. A **291**, 226 (2001).

[9] A. Höll, R. Redmer, G. Röpke, and H. Reinholz, X-ray thomson scattering in warm dense matter, Eur. Phys. J. D **29**, 159 (2004).

[10] S. H. Glenzer, O. L. Landen, P. Neumayer, R. W. Lee, K. Widmann, S. W. Pollaine, R. J. Wallace, G. Gregori, A. Höll, T. Bornath, R. Thiele, V. Schwarz, W.-D. Kraeft, and R. Redmer, Observations of Plasmons in Warm Dense Matter, Phys. Rev. Lett. **98**, 065002 (2007).

[11] E Garcia Saiz, G. Gregori, D. O Gericke, J. Vorberger, B Barbrel, R. J. Clarke, R. R Freeman, S. H. Glenzer, F. Y. Khattak, M Koenig *et al.*, Probing warm dense lithium by inelastic x-ray scattering, Nat. Phys. **4**, 940 (2008).

[12] A. Kietzmann, R. Redmer, M. P. Desjarlais, and T. R. Mattsson, Complex Behavior of Fluid Lithium Under Extreme Conditions, Phys. Rev. Lett. **101**, 070401 (2008).

[13] W. Lorenzen, B. Holst, and R. Redmer, Demixing of Hydrogen and Helium at Megabar Pressures, Phys. Rev. Lett. **102**, 115701 (2009).

[14] U.S. Department of Energy, *Basic Research Needs for High Energy Density Laboratory Physics: Report of the Workshop on High Energy Density Laboratory Physics Research Needs*, Tech. Rep. (Office of Science and National Nuclear Security Administration, 2009).

[15] R. Ernstorfer, M. Harb, C. T Hebeisen, G. Sciaini, T. Dartigalongue, and R. J. Dwayne Miller, The formation of warm dense matter: experimental evidence for electronic bond hardening in gold, Science **323**, 1033 (2009).

[16] E. I. Moses, R. N. Boyd, B. A. Remington, C. J. Keane, and R Al-Ayat, The national ignition facility: Ushering in a new age for high energy density science, Phys. Plasmas **16**, 041006 (2009).

[17] F. M. Bieniosek, J. J. Barnard, A. Friedman, E. Henestroza, J.-Y. Jung, M. A. Leitner, S. Lidia, B. G. Logan, R. M. More, P. A. Ni *et al.*, Ion-beam-driven warm dense matter experiments, in *Journal of Physics: Conference Series*, Vol. 244 (IOP Publishing, Bristol, UK, 2010), p. 032028.

[18] S. Root, R. J. Magyar, J. H. Carpenter, D. L. Hanson, and T. R. Mattsson, Shock Compression of a Fifth Period Element: Liquid Xenon to 840 GPa, Phys. Rev. Lett. **105**, 085501 (2010).

[19] R. F. Smith, J. H. Eggert, R. Jeanloz, T. S. Duffy, D. G. Braun, J. R. Patterson, R. E. Rudd, J. Biener, A. E. Lazicki, A. V. Hamza, J. Wang, T. Braun, L. X. Benedict, P. M. Celliers, and G. W. Collins, Ramp compression of diamond to five terapascals, Nature (London) **511**, 330 (2014).

[20] L. B. Fletcher, H. J. Lee, T. Döppner, E. Galtier, B. Nagler, P. Heimann, C. Fortmann, S. LePape, T. Ma, M. Millot *et al.*, Ultrabright x-ray laser scattering for dynamic warm dense matter physics, Nat. Photonics **9**, 274 (2015).

[21] B. Militzer, Path integral monte carlo and density functional molecular dynamics simulations of hot, dense helium, Phys. Rev. B **79**, 155105 (2009).

[22] K. P. Driver and B. Militzer, First-principles simulations and shock hugoniot calculations of warm dense neon, Phys. Rev. B **91**, 045103 (2015).

[23] T. Schoof, S. Groth, J. Vorberger, and M. Bonitz, *Ab Initio* Thermodynamic Results for the Degenerate Electron Gas at Finite Temperature, Phys. Rev. Lett. **115**, 130402 (2015).

[24] A. Alavi, J. Kohanoff, M. Parrinello, and D. Frenkel, *Ab Initio* Molecular Dynamics with Excited Electrons, Phys. Rev. Lett. **73**, 2599 (1994).

[25] M. W. C. Dharma-wardana and F. Perrot, Simple Classical Mapping of the Spin-Polarized Quantum Electron Gas: Distribution Functions and Local-Field Corrections, Phys. Rev. Lett. **84**, 959 (2000).

[26] N. D. Mermin, Thermal properties of the inhomogenous electron gas, Phys. Rev. **137**, A1441 (1965).

[27] P. Hohenberg and W. Kohn, Inhomogeneous electron gas, Phys. Rev. **136**, B864 (1964).

[28] M. W. C. Dharma-Wardana and R. Taylor, Exchange and correlation potentials for finite temperature quantum calculations at intermediate degeneracies, J. Phys. C: Solid State Phys. **14**, 629 (1981).

[29] M. W. C. Dharma-Wardana and F. Perrot, Density-functional theory of hydrogen plasmas, Phys. Rev. A **26**, 2096 (1982).

[30] F. Perrot and M. W. C. Dharma-wardana, Exchange and correlation potentials for electron-ion systems at finite temperatures, Phys. Rev. A **30**, 2619 (1984).

[31] T. R. Mattsson and M. P. Desjarlais, Phase Diagram and Electrical Conductivity of High Energy-Density Water from Density Functional Theory, Phys. Rev. Lett. **97**, 017801 (2006).

[32] M. D. Knudson, M. P. Desjarlais, A. Becker, R. W. Lemke, K. R. Cochrane, M. E. Savage, D. E. Bliss, T. R. Mattsson, and R. Redmer, Direct observation of an abrupt insulator-to-metal transition in dense liquid deuterium, Science **348**, 1455 (2015).

[33] M. D. Knudson and M. P. Desjarlais, Shock Compression of Quartz to 1.6 TPa: Redefining a Pressure Standard, Phys. Rev. Lett. **103**, 225501 (2009).

[34] M. D. Knudson, M. P. Desjarlais, and A. Pribram-Jones, Adiabatic release measurements in aluminum between 400 and 1200 gpa: Characterization of aluminum as a shock standard in the multimegabar regime, Phys. Rev. B **91**, 224105 (2015).

[35] B. Holst, R. Redmer, and M. P. Desjarlais, Thermophysical properties of warm dense hydrogen using quantum molecular dynamics simulations, Phys. Rev. B **77**, 184201 (2008).

[36] S. M. Wahl, W. B. Hubbard, B. Militzer, T. Guillot, Y. Miguel, N. Movshovitz, Y. Kaspi, R. Helled, D. Reese, E. Galanti *et al.*, Comparing jupiter interior structure models to juno gravity measurements and the role of a dilute core, Geophys. Res. Lett. **44**, 4649 (2017).

[37] B. Militzer and D. M. Ceperley, Path Integral Monte Carlo Calculation of the Deuterium Hugoniot, Phys. Rev. Lett. **85**, 1890 (2000).

[38] V. S. Filinov, M. Bonitz, W. Ebeling, and V. E. Fortov, Thermodynamics of hot dense h-plasmas: Path integral monte carlo simulations and analytical approximations, Plasma Phys. Controlled Fusion **43**, 743 (2001).

[39] T. Schoof, M. Bonitz, A. Filinov, D. Hochstuhl, and J.W. Dufty, Configuration path integral monte carlo, Contrib. Plasma Phys. **51**, 687 (2011).

[40] T. Dornheim, S. Groth, T. Sjostrom, F. D. Malone, W. M. C. Foulkes, and M. Bonitz, Ab Initio, Phys. Rev. Lett. **117**, 156403 (2016).

[41] T. Dornheim, S. Groth, F. D Malone, T. Schoof, T. Sjostrom, W. M.C Foulkes, and M. Bonitz, Ab initio quantum monte carlo simulation of the warm dense electron gas, Phys. Plasmas **24**, 056303 (2017).

[42] W. Kohn and L. J. Sham, Self-consistent equations including exchange and correlation effects, Phys. Rev. **140**, A1133 (1965).

[43] J. C. Smith, A. Pribram-Jones, and K. Burke, Exact thermal density functional theory for a model system: Correlation components and accuracy of the zero-temperature exchange-correlation approximation, Phys. Rev. B **93**, 245131 (2016).

[44] M. A. L. Marques, M. J. T. Oliveira, and T. Burnus, Libxc: A library of exchange and correlation functionals for density functional theory, Comput. Phys. Commun. **183**, 2272 (2012).

[45] V. V. Karasiev, T. Sjostrom, J. Dufty, and S. B. Trickey, Accurate Homogeneous Electron Gas Exchange-Correlation Free Energy for Local Spin-Density Calculations, Phys. Rev. Lett. **112**, 076403 (2014).

[46] S. Groth, T. Dornheim, and M. Bonitz, Free energy of the uniform electron gas: Testing analytical models against first-principles results, Contrib. Plasma Phys. **57**, 137 (2017).

[47] S. Groth, T. Dornheim, T. Sjostrom, F. D. Malone, W. M. C. Foulkes, and M. Bonitz, Ab Initio, Phys. Rev. Lett. **119**, 135001 (2017).

[48] T. Sjostrom and J. Daligault, Gradient corrections to the exchange-correlation free energy, Phys. Rev. B **90**, 155109 (2014).

[49] V. V. Karasiev, J. W. Dufty, and S. B. Trickey, Nonempirical Semilocal Free-Energy Density Functional for Matter under Extreme Conditions, Phys. Rev. Lett. **120**, 076401 (2018).

[50] D. J. Carrascal, J. Ferrer, J. C. Smith, and K. Burke, The hubbard dimer: a density functional case study of a many-body problem, J. Phys.: Condens. Matter **27**, 393001 (2015).

[51] A. J. Cohen and P. Mori-Sánchez, Landscape of an exact energy functional, Phys. Rev. A **93**, 042511 (2016).

[52] J. I. Fuks, M. Farzanehpour, I. V. Tokatly, H. Appel, S. Kurth, and A. Rubio, Time-dependent exchange-correlation functional for a hubbard dimer: Quantifying nonadiabatic effects, Phys. Rev. A **88**, 062512 (2013).

[53] J. I. Fuks and N. T. Maitra, Charge transfer in time-dependent density-functional theory: Insights from the asymmetric hubbard dimer, Phys. Rev. A **89**, 062502 (2014).

[54] J. I. Fuks and N. T. Maitra, Challenging adiabatic time-dependent density functional theory with a hubbard dimer: the case of time-resolved long-range charge transfer, Phys. Chem. Chem. Phys. **16**, 14504 (2014).

[55] V. Turkowski and T. S Rahman, Nonadiabatic time-dependent spin-density functional theory for strongly correlated systems, J. Phys.: Condens. Matter **26**, 022201 (2014).

[56] D. J. Carrascal, J. Ferrer, N. Maitra, and K. Burke, Linear response time-dependent density functional theory of the Hubbard dimer, Eur. Phys. J. B **91**, 142 (2018).

[57] K. Deur, L. Mazouin, and E. Fromager, Exact ensemble density functional theory for excited states in a model system: Investigating the weight dependence of the correlation energy, Phys. Rev. B **95**, 035120 (2017).

[58] K. Burke, J. C. Smith, P. E. Grabowski, and A. Pribram-Jones, Exact conditions on the temperature dependence of density functionals, Phys. Rev. B **93**, 195132 (2016).

[59] M. Herrera, K. Zawadzki, and I. D'Amico, Melting a Hubbard dimer: Benchmarks ofalda'for quantum thermodynamics, arXiv:1803.06724.

[60] E. Kamil, R. Schade, T. Pruschke, and P. E. Blöchl, Reduced density-matrix functionals applied to the hubbard dimer, Phys. Rev. B **93**, 085141 (2016).

[61] K. Schönhammer, O. Gunnarsson, and R. M. Noack, Density-functional theory on a lattice: Comparison with exact numerical results for a model with strongly correlated electrons, Phys. Rev. B **52**, 2504 (1995).

[62] A. Cangi, E. K. U. Gross, and K. Burke, Potential functionals versus density functionals, Phys. Rev. A **88**, 062505 (2013).

[63] A. Cangi and A. Pribram-Jones, Efficient formalism for warm dense matter simulations, Phys. Rev. B **92**, 161113 (2015).

[64] W. Yang, P. W. Ayers, and Q. Wu, Potential Functionals: Dual to Density Functionals and Solution to the v-Representability Problem, Phys. Rev. Lett. **92**, 146404 (2004).

[65] A. Cangi, D. Lee, P. Elliott, K. Burke, and E. K. U. Gross, Electronic Structure Via Potential Functional Approximations, Phys. Rev. Lett. **106**, 236404 (2011).

[66] See Supplemental Material at http://link.aps.org/supplemental/10.1103/PhysRevB.98.075148 for a thorough derivation of the XC free energy equations and numerical demonstrations of the approximations.

[67] E. W. Brown, B. K. Clark, J. L. DuBois, and D. M. Ceperley, Path-Integral Monte Carlo Simulation of the Warm Dense Homogeneous Electron Gas, Phys. Rev. Lett. **110**, 146405 (2013).

[68] F. D. Malone, N. S. Blunt, E. W. Brown, D. K. K. Lee, J. S. Spencer, W. M. C. Foulkes, and J. J. Shepherd, Accurate Exchange-Correlation Energies for the Warm Dense Electron Gas, Phys. Rev. Lett. **117**, 115701 (2016).